# An Extended Minimum Spanning Tree method for characterizing local urban patterns

Bin Wu, Bailang Yu, Qiusheng Wu, Zuoqi Chen, Shenjun Yao, Yan Huang & Jianping Wu

Published online: 04 Oct 2017.

Submit your article to this journal ☐

View related articles ☐

View Crossmark data ☐

Taylor & Francis
Taylor & Francis Group

ARTICLE

Check for updates

# An Extended Minimum Spanning Tree method for characterizing local urban patterns

Bin Wu[a,b], Bailang Yu [a,b], Qiusheng Wu [c], Zuoqi Chen[a,b], Shenjun Yao[a,b], Yan Huang[a,b] and Jianping Wu[a,b]

[a]Key Laboratory of Geographic Information Science (Ministry of Education), East China Normal University, Shanghai, China; [b]School of Geographic Sciences, East China Normal University, Shanghai, China; [c]Department of Geography, Binghamton University, State University of New York, Binghamton, NY, USA

**ABSTRACT**

Detailed and precise information on urban building patterns is essential for urban design, landscape evaluation, social analyses and urban environmental studies. Although a broad range of studies on the extraction of urban building patterns has been conducted, few studies simultaneously considered the spatial proximity relations and morphological properties at a building-unit level. In this study, we present a simple and novel graph-theoretic approach, Extended Minimum Spanning Tree (EMST), to describe and characterize local building patterns at building-unit level for large urban areas. Building objects with abundant two-dimensional and three-dimensional building characteristics are first delineated and derived from building footprint data and high-resolution Light Detection and Ranging data. Then, we propose the EMST approach to represent and describe both the spatial proximity relations and building characteristics. Furthermore, the EMST groups the building objects into different locally connected subsets by applying the Gestalt theory-based graph partition method. Based on the graph partition results, our EMST method then assesses the characteristics of each building to discover local patterns by employing the spatial autocorrelation analysis and homogeneity index. We apply the proposed method to the Staten Island in New York City and successfully extracted and differentiated various local building patterns in the study area. The results demonstrate that the EMST is an effective data structure for understanding local building patterns from both geographic and perceptual perspectives. Our method holds great potential for identifying local urban patterns and provides comprehensive and essential information for urban planning and management.

## 1. Introduction

In recent decades, the amount of the earth's surface covered by urban areas has expanded enormously with the development of modern society. The rapid urbanization not only promotes urban expansions and sprawls but also makes the function, structure and morphology of cities increasingly diverse and complex (Whitehand 1992, Lowry and Lowry 2014). Various urban features, such as buildings, trees, streets, parking lots and open spaces, structure and shape cities into a multidimensional urban form. Through

the analysis of the spatial structure and characteristics of urban forms, the ongoing urban structures and complex built environments can be better understood. Moreover, appreciation of the complex urban morphology also helps urban planner to be aware of local patterns of development and the evolution of urban spaces, and hence gain more insights to enhance the design of new urban layouts (Donnay *et al.* 2003). Therefore, novel solutions for interpretation and analysis of the spatial pattern of urban features are of great importance (de Almeida *et al.* 2013).

Among all urban features, buildings are one of the most crucial components of urban structures and functions (Yoshida and Omae 2005, Steiniger *et al.* 2008). Detailed and precise information on buildings, especially building patterns, are essential for understanding and characterizing urban and other built-up spaces (Carmona *et al.* 2003, Du *et al.* 2016). In addition, building patterns can be used to evaluate landscape configuration (Yoshida and Omae 2005) and estimate urban population (Wu *et al.* 2005). The definition of building patterns varies greatly in different research fields. Regarding building functions, they can be divided into three categories: single-family, multifamily and nonresidential buildings according to Meinel *et al.* (2009). Some studies (Mesev 2005, Steiniger *et al.* 2008) further inferred the urban structures, for example, industry/commercial, inner city, suburban and rural area, from these building patterns. In the field of building typification and map generalization, building patterns can be categorized into many different patterns with special structures such as linear (straight), circular, star and other irregular patterns (Regnauld 2001, Christophe and Ruas 2002, Li *et al.* 2004, Anders 2006, Zhang *et al.* 2013a, 2013b, Du *et al.* 2016). Building patterns are also referred to as spatially homogeneous or heterogeneous and locally connected units that link each building to its neighbors (Gans 1961, Cadenasso *et al.* 2007, Baud *et al.* 2010, Caruso *et al.* 2017). Although different studies have different emphasis on building patterns, the basic principle for extracting building patterns is similar, in which building patterns are typically regarded as local groups of buildings with similar geometric, semantic, structural and spatial characteristics between them (Christophe and Ruas 2002, Cetinkaya *et al.* 2015), which indicates that urban building patterns can be derived from the intrinsic attributes of buildings and the inter-building characteristics.

Building patterns are hidden in urban areas with a lot of unstructured and unordered buildings. Thus efficient and effective methods are required to recognize and extract them. Many studies (Regnauld 2001, Christophe and Ruas 2002, Li *et al.* 2004, Cetinkaya *et al.* 2015, Caruso *et al.* 2017) pointed out that the spatial proximity relations between buildings are the foundation of building pattern analysis. This argument can be supported by two aspects. From a geographic perspective, Tobler's first law of Geography says that 'everything is related to everything else, but near things are more related than distant things' (Tobler 1970). The law suggests that close buildings may be more spatially dependent or associated with each other. From a cognitive psychology aspect, people are inclined to visually perceive close objects as groups according to the Gestalt principles (Nordbeck 1971, Li *et al.* 2004, Sternberg and Sternberg 2011, Yu *et al.* 2014, Cetinkaya *et al.* 2015). Therefore, the identification of the proximity relationships among buildings can further reveal the hidden building patterns.

Various methods have been reported in the literature to analyze urban building patterns according to the spatial proximity relations. In general, these methods can be grouped into several categories (Han *et al.* 2009, Deng *et al.* 2011): partitioning, hierarchical, density-based, grid-based and graph-based methods. In addition to these

methods, some studies analyzed building patterns by applying the space syntax (Ratti 2004) and periodicity analysis (Dogrusoz and Aksoy 2007b). Among these methods, the graph-based approaches are particularly popular and appealing because they preserve both the structural information and proximities of buildings (Cetinkaya *et al.* 2015, Caruso *et al.* 2017). Furthermore, the graph-based approaches can be easily applied to large areas with a few inputs. Many different types of graphs, such as the relative relation graph (Anders *et al.* 1999), Minimum Spanning Tree (MST) (Regnauld 1996, 2001), neighborhood graph (Walde *et al.* 2014), Delaunay triangulation and Voronoi graph (Li *et al.* 2004, Dogrusoz and Aksoy 2007a), have been successfully utilized.

The MST is probably one of the most widely used graph-based algorithms for building pattern identification. Regnauld (2001) generated MST graphs from the centroids of buildings, and then obtained subgroups of buildings by eliminating inconsistent edges based on various criteria taken from the Gestalt theory. Based on such analysis, each group of buildings is attached with essential geographical information, for example, the average size of buildings, shape of the group and density, among others. Dogrusoz and Aksoy (2007a) classified buildings into organized or unorganized groups by constructing MST graphs through Voronoi tessellation of the IKONOS image. Zhang *et al.* (2013a) recognized building patterns from topographic data by producing MST from constrained Delaunay triangulation and by removing inconsistent edges of the MST based on proximity property. Caruso *et al.* (2017) used an MST to identify urban local building patterns by measuring the local index of spatial association on inter-building distances. However, these existing approaches mainly focused on the spatial arrangement and alignment of buildings, which have been tailored to extract special patterns instead of the meaningful local homogeneous units. Moreover, only the distance between buildings and a few shape metrics were taken into account in the determination of building patterns. Many studies (Anders *et al.* 1999, Regnauld 2001, Donnay *et al.* 2003, Li *et al.* 2004, Yu *et al.* 2010) argued that the two-dimensional (2D) and three-dimensional (3D) building morphological information, namely, urban building characteristics (UBCs), such as height, volume, size and orientation, are essential for building pattern analysis. Therefore, novel solutions for building pattern investigation are especially needed that can take both 2D and 3D UBCs into account.

To better understand and interpret urban forms, GIS (geographical information systems) and remote sensing techniques have been widely used to infer UBCs and spatial structures (Mesev 2005, Grinias *et al.* 2016). As one of the most attractive remote sensing techniques for urban information extraction, Light Detection and Ranging (LiDAR) can provide highly accurate and dense 3D point clouds of urban objects (Yu *et al.* 2009, 2016, Brodu and Lague 2012, Wu *et al.* 2012, 2013, 2016a, Huang *et al.* 2015, Liu and Lim 2016). Among the various LiDAR platforms, airborne LiDAR has been widely used for extracting urban building information (Zhang *et al.* 2006, Sohn and Dowman 2007, Yu *et al.* 2010, Wu *et al.* 2017). From airborne LiDAR data, planimetric attributes, shape attributes and volumetric attributes of each building, such as the building footprint, height, volume, floor area ratio and density, can be calculated (Sohn and Dowman 2007, Liu *et al.* 2010, Yu *et al.* 2010, Niemeyer *et al.* 2014, Wu *et al.* 2016b). The building information provides a direct and objective measure of the physical morphology of urban buildings, which are essential for understanding the urban built space and settlement systems (Zhang *et al.* 2006, Chen *et al.* 2009). By fusing the detailed and specific information derived from airborne LiDAR into building pattern analysis, more meaningful spatially homogeneous or heterogeneous units can be discovered.

In this paper, we present a flexible graph-based data structure, Extended Minimum Spanning Tree (EMST), to describe and represent the spatial proximity relations and multi-dimensional UBCs among building objects. The building objects are delineated and derived from building footprint data and high-resolution airborne LiDAR data, which provide abundant 2D and 3D morphologic information for each building. Based on these meaningful building objects, the local building subsets and spatially homogeneous or heterogeneous units at building-unit level are identified by the proposed EMST. This study has three objectives: (1) to extract meaningful building objects; (2) to establish the data structure of the EMST; and (3) to conduct building pattern analysis based on our EMST approach at building-unit level. The paper is structured as follows: Section 2 introduces the study area and datasets. The data processing and methodology are presented in Section 3. Section 4 presents the results of our case study, along with a discussion in Section 5. Finally, the conclusion and an outlook on the next steps of our work are given in Section 6.

## 2. Study area and data

Our study area, Staten Island (Figure 1(a)), is one of the five boroughs of New York City in the U.S. state of New York. Located in the southernmost part of New York City and the state of New York, Staten Island has the third-largest inland area of 152 km$^2$ among the five boroughs. According to the United States Census Bureau (2016), it has a population of more than 0.47 million in 2016. Staten Island is mostly flat and has an average elevation of 23 m above sea level. The North Shore is the most urbanized part of the island, while the South Shore is mostly suburban. The West Shore is the least populated but most industrial part of the island. The uneven distribution of buildings and various building shapes/types make the Staten Island a great place for validating our proposed method.

The airborne LiDAR data were distributed by the U.S. Geological Survey (USGS), which can be downloaded from the OpenTopography Facility website (http://opentopo.sdsc.edu/datasets?id=OTEXT.062015.26918.1&host=community, Accessed May 2017). According to
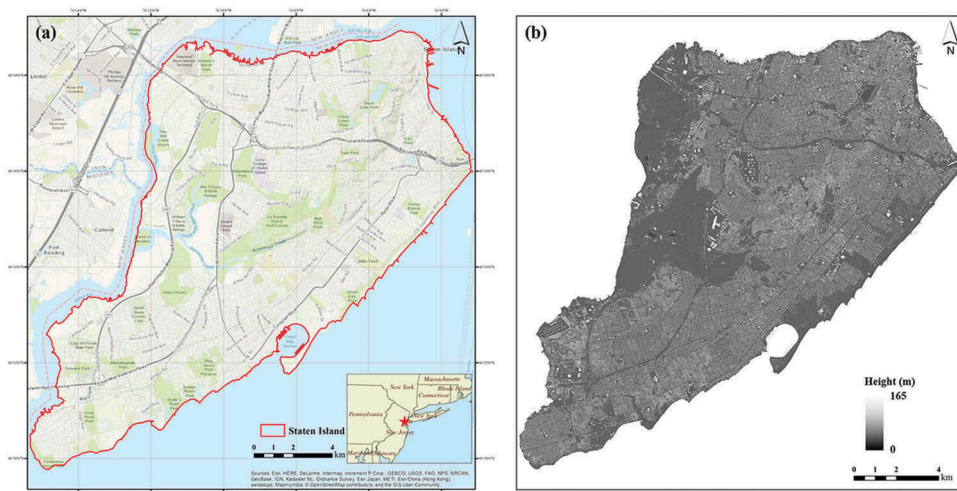


**Figure 1.** Case study area and data. (a) Geographical location of Staten Island; (b) Normalized Digital Height Model (nDSM) derived from airborne LiDAR data.

the metadata, the LiDAR data were collected using a Leica ALS70 LiDAR system from August 2013 to April 2014. The downloaded LiDAR LAS files had been processed and classified as ground and non-ground points by the USGS. The point cloud extracted for the study area consists of approximately one billion LiDAR points with a point density of 7.76 points/m². The LiDAR data were processed and projected in Universal Transverse Mercator Zone 18, North American Datum of 1983 in unit of meters. The vertical datum was referenced to North American Vertical Datum of 1988 (NAVD 88), GEOID 12A, in unit of meters.

The building footprint in vector format of New York City was released by the NYC Department of Information Technology and Telecommunications (DoITT, http://www1.nyc.gov/site/doitt/index.page, Accessed May 2017) and delivered as an ESRI geodatabase. The building footprint data used in our study were captured and updated in 2016 based on the 2014 aerial photography by the NYC DoITT building editors. In total, 103,901 buildings in our study area were extracted from the NYC DoITT geodatabase. The data record the basic information of buildings, including building identification number, number of floors and the year of construction.

## 3. Methodology

### 3.1. *Data preprocessing*

In order to obtain accurate 3D building morphologic information, we generated the Normalized Digital Height Model (nDSM) from the LiDAR point cloud. First, a Digital Surface Model (DSM) was interpolated from all the LiDAR points by using the linear Triangulated Irregular Network (TIN) interpolation method. As noted in Section 2, the LiDAR points had already been classified into ground and non-ground points. We then extracted the LiDAR points labeled as ground to generate the Digital Elevation Model (DEM) by using the linear TIN interpolation method as well. By subtracting the DEM grid from the DSM grid, the nDSM grid was created. The cell size for the DSM, DEM and nDSM was determined using the following equation according to previous studies (Chen *et al.* 2006, Wu *et al.* 2016b, 2017):

$$c = \sqrt{1/n} \tag{1}$$

where *n* is the LiDAR pulse density (returns/m²). Based on Equation (1), the cell size for the DSM, DEM and nDSM in our study was set to 0.5 m. Since data noise or errors may exist in the nDSM, a standard Gaussian smoothing filter was used to smooth the nDSM grid (Wu *et al.* 2016b, 2017). Figure 1(b) shows the smoothed nDSM data for the entire Staten Island.

### 3.2. *Building object extraction*

The object-based model has been widely used and studied in the domain of urban studies. Many studies argued that the object-based model is the most effective data structure, which is more in line with the way to interpret the urban scene by humans or computers (Miliaresis and Kokkas 2007, Antonarakis *et al.* 2008, Liu *et al.* 2010, Taubenböck *et al.* 2010, Yu *et al.* 2010). Based on the object-based model, the knowledge of the constituent elements of the urban scene (e.g. the size and shape of buildings) can be revealed (Neuwirth *et al.* 2016). In this study, we treated buildings as
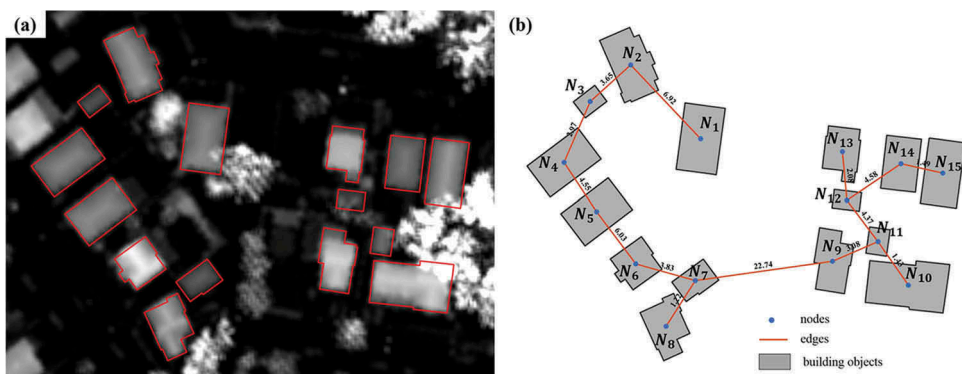
**Figure 2.** Representation of minimum spanning tree. (a) Building objects overlaid on nDSM; (b) minimum spanning tree based on the minimum distance between buildings' boundaries.

objects. Before building objects can be measured and described, they must first be identified and delineated. Since we already have the building footprint vector data and they match very well with the nDSM data (see Figure 2(a)), the delineation of buildings from the nDSM is not needed. The boundary of each building object is the same as the corresponding polygon feature in the NYC DoITT geodatabase. Therefore, the creation of building objects can be simplified as the following two steps. The first step is to assign object identifiers. In order to distinguish a building object from others, a unique ID number is assigned to each building object. The next step is to derive building characteristics of each building object. The building characteristics measure various aspects of building attributes, including planimetric attributes, shape attributes and volumetric attributes, which can be simply divided into 2D and 3D measures. In this way, the original building footprint data are successively transformed into more meaningful building objects that better correspond to the visual perception of humans (Burnett and Blaschke 2003, Benz *et al.* 2004, Yu *et al.* 2010).

The building footprint vector data and the smoothed LiDAR nDSM enable the calculation of various UBCs for building objects. The building footprint vector data were mainly used for calculating 2D attributes, while the LiDAR nDSM was mainly utilized for deriving 3D attributes. A total of 13 UBCs were selected and extracted in this study, which are summarized in Table 1. These UBCs are the commonly used attributes in urban studies (Yoshida and Omae 2005, Steiniger *et al.* 2008, Yu *et al.* 2010, 2014, 2017, Berger *et al.* 2017). The size of a building is described by calculating the area ($A$), perimeter ($P$), width ($w$) and length ($l$) of the building. The shape of a building is described by four indices: orientation ($\phi$), compactness index ($CI$), elongatedness ($ELG$) and rectangularity ($REC$). Height ($H$), average height ($\bar{H}$), volume ($V$) and average volume per floor ($\bar{V}$) are used to describe the volumetric attributes of buildings.

## 3.3. *Extended Minimum Spanning Tree*

Graph theory is a popular way to represent the relationship among a set of urban building objects. Many studies have illustrated the power and potential utility of applying graph theory for urban pattern analysis (Urban and Keitt 2001, Assunção *et al.* 2006,

**Table 1.** Definitions of 2D and 3D attributes for building objects.

| Attributes | Definition |
|---|---|
| **2D** centroid point | The 2D geometric center of a building object. |
| **Area** (*A*) | The areal extent of a building object. |
| **Perimeter** (*P*) | The distance around a building object. |
| **Length** (*l*) | The length of the minimum bounding rectangle enclosing the building object (see Figure 3). |
| **Width** (*w*) | The width of the minimum bounding rectangle enclosing the building object (see Figure 3). |
| **Orientation** ($\phi$) | The angle in degree between the *x*-axis and the major axis of the minimum bounding rectangle measured counterclockwise (see Figure 3). |
| **Compactness index** (*CI*) | $CI = \frac{4\pi A}{P^2}$ |
| **Elongatedness** (*ELG*) | $ELG = \frac{l}{w}$ |
| **Rectangularity** (*REC*) | $REC = \frac{A}{lw}$ |
| **Height** (*H*) | $H = max_{i=1}^{n}(h_i)$ |
| **Average height** ($\bar{H}$) | $\bar{H} = \frac{\sum_{i=1}^{n} h_i}{n}$ |
| **Volume** (*V*) | $V = r^2 \sum_{i=1}^{n} h_i$ |
| **Average volume per floor** ($\bar{V}$) | $\bar{V} = \frac{r^2 \sum_{i=1}^{n} h_i}{f}$ |

*r* is the cell size of nDSM, *n* is the number of cells enclosed by a building object, $h_i$ is the height value from nDSM of *i* th cell in the building object, *f* is the number of floors.

Dogrusoz and Aksoy 2007a, Yu *et al*. 2014). In general, a simple graph *G* consists of a finite, non-empty set of nodes *N*(*G*) and edges *E*(*G*). Meanwhile, each edge $E_{ij}(N_i, N_j)$ connects nodes $N_i$ and $N_j$ in graph *G*.

In urban applications, each member of the set *N*(*G*) in graph *G* corresponds to a unique urban object, and an edge $E_{ij}(N_i, N_j)$ between nodes $N_i$ and $N_j$ indicates that a relation exists between the corresponding urban objects. Additional attributes describing each node can be included in the graph. For example, in landscape applications, the nodes commonly represent landscape patches defined as discrete areas with homogeneous environmental conditions, and each node can be located by its spatial centroid and
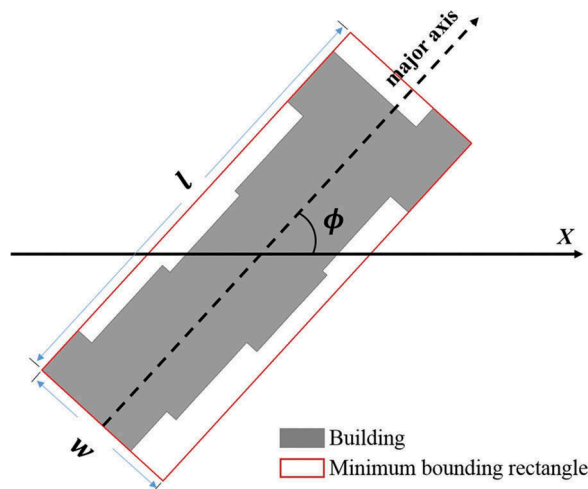


**Figure 3.** Illustration of minimum bounding rectangle enclosing a building object.

described by its area. Therefore, each edge in the graph has its weight, which can be calculated from the corresponding two adjacent nodes. The weight can either be the distance between the nodes, or described by some other features. So, these graphs are also considered as weighted graphs. In a weighted graph, each node is reachable from some other nodes. A spanning tree of a weighted graph $G$ is defined as a subgraph of $G$ which connects all nodes of $G$. Generally, a graph $G$ can have multiple spanning trees with different total weight. Among the various spanning trees, the spanning tree of $G$ with the smallest total weight is defined as the MST. Since MSTs can be computed quickly and they can provide a simple way to identify clusters in a set of nodes, they have long been of interest in urban studies (Urban and Keitt 2001, Caruso et al. 2017). Moreover, some connected urban components or local clusters can be inferred and detected by pruning the MST graph.

The simple MSTs, however, could not represent the spatial relations and various UBCs of building objects simultaneously. By extending the MST to allow the representation of various UBCs, it is possible to derive a more complete description of urban forms from different perspectives. More importantly, the local patterns of buildings can be captured by extending the capacity of MST to incorporate the power of some graph operations and spatial association analysis. In this study, we have extended the basic MST, $G$, to incorporate some additional series of sets. We referred to this new data model as the EMST. The main advantage of EMST over the basic MST is that it provides a more complete, formal, and explicit sets, relations, and functions to describe the spatial relation and structure of urban objects. In the EMST, the relations and properties are divided into logical groups. The formal description of EMST can be represented as follows:

$$EMST = \{N, E, W, A, C, S, P\} \tag{2}$$

where $N$ is the set of nodes, $E$ is the set of edges, $W$ is the set of edge weight recording the length of the edge, $A$ is the set of various properties associated with the nodes in $N$, $C$ is the set of subgraphs, $S$ is the set describing the statistical results for each group in $C$ and $P$ is the set of local pattern units. In Equation (2), the sets of $N$, $E$ and $W$ are the standard elements of the basic MST. The additional four sets (i.e. $A$, $C$, $S$ and $P$) are the newly added logical groups created according to the information they represent. Each of these newly added sets is discussed in detail later.

Before describing these additional sets, the generation of MST is introduced first. In our study, the nodes represent buildings which are located by their centroid point, and the edges represent the proximal relations of buildings. Because buildings are represented as 2D objects with various size and shape on a map, it is critical that the proximity between building objects is measured by the distance between their boundaries rather than by the distance between their centroid points (Yu et al. 2014). Therefore, only the distance between adjacent building boundaries, not the distance between adjacent centroid points, is considered as the unitary cost to build the MST by using the Prim's algorithm (Prim 1957). Each node in the MST is indexed by its corresponding building object and labeled with the building object ID. Figure 2(b) shows the basic MST constructed for the building objects in Figure 2(a).

### 3.3.1. *Representation of building properties set* A

As illustrated in Section 3.2, the UBCs of building objects are important because they provide essential information about the nature of buildings in urban areas. In this study, each UBC in Table 1 is stored as a single numerical value except the centroid point, which is implied in the nodes set $N$. In EMST, these UBCs are represented by the set $A$. Thus, the set $A$ can be represented by

$$A = \{a_1, a_2, \ldots, a_m\} \tag{3}$$

where $a_i$ represents the $i$ th ($0 \leq i < m$) UBC and $m$ is the total number of UBCs. Given this equation, we can locate the $i$th ($0 \leq i < m$) UBC of the $j$ th ($N_j$) node in $N$. To be more specific, the representation of the UBCs of a node $N_j$ can be characterized by a vector which has the general form of

$$A_{N_j} = \{a_{j1}, a_{j2}, \ldots, a_{jm}\} \tag{4}$$

Similarly, the representation of the UBCs for all the nodes in EMST has a matrix characterization of

$$A_{ALL} = \begin{pmatrix} a_{11} & \cdots & a_{1m} \\ \vdots & \ddots & \vdots \\ a_{i1} & \cdots & a_{ij} \end{pmatrix} \tag{5}$$

### 3.3.2. *Representation of subgraphs set* C

The MST for a study region might be too large and complex to analyze and discover the local patterns. Hence, we subdivided the MST graph into many subgraphs. In EMST, we applied the Gestalt theory-based method to partition the MST appropriately into different subgraphs. After the MST construction, the weight $W_{ij}$ for an edge $E_{ij}$ is represented by the minimum boundary distance between building object $N_i$ and $N_j$. According to the Gestalt theory, the principle for the MST partition process is to find the edge with a heavy weight significantly different from its neighbors. Here, we adopted the method proposed by Yu *et al.* (2014), which used the ratio ($\tau$) of the weight difference between $W_{ij}$ for edge $E_{ij}$ and the average weight of its nearby edges to the standard deviation of those edges' weights. An edge is considered to be inconsistent and then cut off from the MST if the ratio is larger than a given threshold ($\tau_0$). As noted earlier, nearby edges are used to calculate the standard deviation and average of weights for each node object in edge $E_{ij}$. In fact, these nearby edges are defined as the ones within a specific step length to a certain node. To assist in the understanding of the method, a simple example is presented in Figure 4(a). As shown in Figure 4(a), the edges $E_{6,7}(N_6, N_7)$ and $E_{7,8}(N_7, N_8)$ are within one step to node $N_7$. Similarly, the edge $E_{5,6}(N_5, N_6)$ is within two steps to node $N_7$. The step length and the ratio threshold ($\tau_0$) are both set to 2 according to Yu *et al.* (2014).

After removing the inconsistent edges based on the earlier rules, the MST is divided into many subgraphs. Assuming that the edge $E_{7,9}(N_7, N_9)$ shown in Figure 4(a) is identified as an inconsistent edge, the MST will be separated into two subgraphs and the result is shown in Figure 4(b). In EMST, these subgraphs are stored by the set $C$. The set $C$ has a general form of

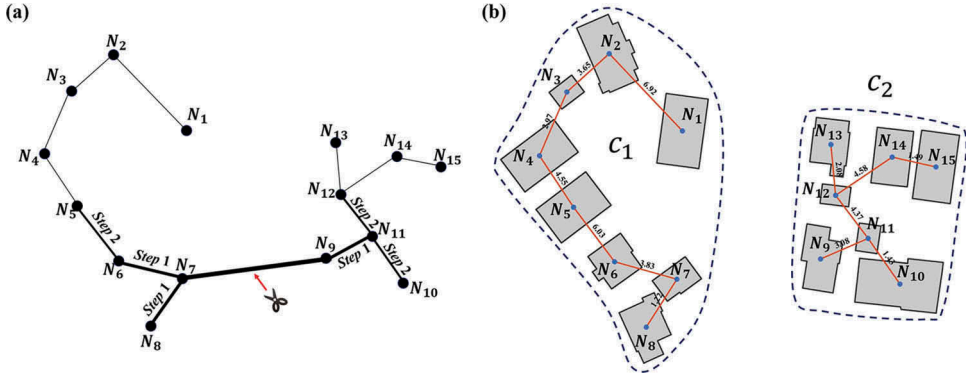$$C = \{c_1, c_2, \ldots, c_i\} \tag{6}$$

**Figure 4.** MST partition. (a) Definition of nearby edges by steps; (b) subgraphs after removing the inconsistent edge.

where each $c \in C$ denotes a subgraph. It should be noted that each $c \in C$ is comprised of several nodes and edges which has the form of

$$c_i = \{N^{c_i}, E^{c_i}, W^{c_i}\} \tag{7}$$

where $N^{c_i}, E^{c_i}, W^{c_i}$ refer to the set of nodes, edges and weights, respectively. For example, subgraph $c_1$ in Figure 4(b) has eight nodes and seven edges, which can be described as

$$c_1 = \{N^{c_1}, E^{c_1}, W^{c_1}\} = \left\{ \begin{array}{c} \{N_1, N_2, N_3, N_4, N_5, N_6, N_7, N_8\}, \{E_{1,2}, E_{2,3}, E_{3,4}, E_{4,5}, E_{5,6}, E_{6,7}, E_{7,8}\}, \\ \{6.92, 3.65, 2.97, 4.55, 6.03, 3.83, 1.22\} \end{array} \right\}. \tag{8}$$

### 3.3.3. Representation of the statistical results set $S$

For each subgraph, five statistical indicators, i.e. maximum (*max*), minimum (*min*), average (*avg*), median (*med*) and standard deviation (*std*), are calculated for each UBC in set $A$. These statistical indicators are very important for understanding the building information at a local level. The set $S$ has the form

$$S = \{\{max^{c_1}, min^{c_1}, avg^{c_1}, med^{c_1}, std^{c_1}\}, \ldots, \{max^{c_i}, min^{c_i}, avg^{c_i}, med^{c_i}, std^{c_i}\}\} \tag{9}$$

Equation (9) states that $S$ comprises a series of subsets, each of which has five elements recording the statistical results for its corresponding subgraph.

### 3.3.4. Representation of the local pattern unit set $P$

We argue that when the buildings are very close to each other in a subgraph, the building boundary distance is not sufficient to reflect the local pattern of buildings. In order to include multi-perspective views on local building patterns at a building-unit level, we further investigate the homogeneous and heterogeneous units for each subgraph by integrating the UBCs set and Local Indicator of Spatial Association (LISA). This also means that we consider local statistics as a descriptor of pattern rather than graph cutting in subgraphs at this stage. Anselin (1995) used LISA to identify clusters of similar values in space and this method has been widely used in the socioeconomic applications (Fan and Myint 2014). As the most popular LISA, the local Moran's $I$ index measures the degree of spatial autocorrelation as the weighted product of the difference to the mean of the value

of a variable at a certain observation and the same difference for all other observations, with more weight given to the observations in close spatial proximity. Local Moran's $I$ index $I_i$ for node $N_i$ within a given subgraph of the MST can be expressed as

$$I_i = \frac{z_i - \bar{z}}{\delta^2} \sum_{j=1, j\neq i}^{n} \omega_{ij}(z_j - \bar{z}) \tag{10}$$

where $z_i$ and $z_j$ are the value of the specific UBC at node $i$ and node $j$, respectively (where $j \neq i$); $\bar{z}$ is the mean value of $z$ with the sample number of $n$; $\delta^2$ is the variance of $z$; and $\omega_{ij}$ is a pairwise weighting parameter indicating the proximity of node $i$ and node $j$. Here, the weight $\omega_{ij}$ is different from the weight matrix in EMST and is determined using a distance threshold: nodes (building objects) within a distance band are given the same weight of 1, while those outside the distance band are given the weight of 0. According to previous studies (Nordbeck 1971, Donnay *et al*. 2003, Caruso *et al*. 2017), the distance band was set to 200 m.

A significant positive local Moran's $I$ value implies that the node $N_i$ is surrounded by nodes with a similar $z$ value, and these nodes are considered as locally homogeneous units with respect to the $z$ indicator. Two local homogeneous pattern units, high-high patterns (high values surrounded by high value neighborhood) and low-low patterns (low values surrounded by low value neighborhood) are included. In contrast, a significant negative local Moran's $I$ value means that the $z$ value of the node $N_i$ is obviously different from its surrounding nodes, which implies a potential heterogeneous pattern. Similarly, there are two heterogeneous situations, which include high-low (a high value surrounding by low value neighborhood) and low-high (a low value surrounding by high value neighborhood). In addition, there is no specific pattern if Moran's $I$ is not significant, which was also treated as a heterogeneous unit. Thus, the set $P$ has the form

$$P = \{p_1, p_2, \ldots, p_i\} \tag{11}$$

where each $p \in P$ records the local pattern units in a subgraph. Each $p \in P$ is comprised of five local patterns and has the form

$$p_i = \{HH^{c_i}, LL^{c_i}, HL^{c_i}, LH^{c_i}, NS^{c_i}\} \tag{12}$$

where $HH^{c_i}$, $LL^{c_i}$, $HL^{c_i}$, $LH^{c_i}$ and $NS^{c_i}$ refer to the nodes and edges set of high-high, low-low, high-low, low-high and nonsignificant local pattern units in subgraph $c_i$.

### 3.4. *Homogeneity index*

Based on the EMST, the local homogeneous and heterogeneous units of each UBC can be identified. In order to measure the overall homogeneity degree, we propose a homogeneity index. Let

$$J(e^{c_i}|a_j) = \begin{cases} 1 \text{ if } e^{c_i} \in HH^{c_i} \text{ or } LL^{c_i} \\ 0 \text{ otherwise} \end{cases} \tag{13}$$

where $e^{c_i}$ is the edge of $c_i$, $a_j$ is the $j$th UBC. This means that $J(e^{c_i}|a_j)$ of edge $e^{c_i}$ becomes 1 if the edge $e^{c_i}$ is located in the homogeneous set $HH^{c_i}$ or $LL^{c_i}$. Otherwise, it becomes 0. In terms of all the UBCs, we define the homogeneity index $hi$ as

$$hi(e^{c_i}) = \sum_{j=1}^{m} J(e^{c_i}|a_j) \tag{14}$$

where $m$ is the number of UBCs. In fact, the homogeneity index refers to the times that $J(e^{c_i}|a_j)$ equals to 1 when $j$ ranges from 1 to $m$. If edge $e^{c_i}$ belongs to homogeneous set for all the UBCs, then $hi(e^{c_i}) = m$; if edge $e^{c_i}$ does not belong to any homogeneous sets for all the UBCs, then $hi(e^{c_i}) = 0$. A high homogeneity index indicates that the corresponding two buildings linked by the edge have many building characteristics in common. The higher homogeneity index is, the more similar they are. By mapping the distribution of homogeneity index, the overall building patterns can be characterized.

## 4. Results

Having established the methodology, we applied our method to investigate the local building patterns over the Staten Island. We first created an nDSM grid with 0.5 m cell size from the LiDAR point cloud and extracted 103,901 building footprints from the NYPI geodatabase. Then, all the 13 UBCs were computed for each building object from the smoothed LiDAR nDSM data and the footprint vector data by using the calculation method introduced in Table 1. Summary statistics on these UBCs of all the building objects in our study area are presented in Table 2. The buildings on the Staten Island have a mean area of approximately 120 m$^2$ and a mean perimeter of approximately 44 m. The high standard deviations of area and perimeter measures indicate that the buildings in the study area are spread out over a wider range of size. Based on the geometric attributes, most of the buildings have a rectangular shape with a mean *REC* value of 0.93 and a very low standard deviation of 0.10. From the statistics of 3D morphological indices, these buildings have an average height of 7.56 m, which occupies an average volume of 812 m$^3$ and an average volume of 584 m$^3$ per floor. It is worth noting that the standard deviations of volume and volume per floor are very high in the study area, which is partly due to the many large buildings in the study area, such as townhouse, apartment and factories. These UBCs can help enhance the understanding of the buildings in this area statistically.

Based on the building objects, we constructed the EMST structure as described in Section 3.3 for the entire study area. All the computations were conducted on a consumer-level PC with an Intel Core i7 3.0 GHz CPU, 16 GB RAM, running Windows 7

**Table 2.** Summary statistics on urban building characteristics in the study area.

| UBCs | Min | Median | Mean | Max | Standard deviation |
|---|---|---|---|---|---|
| $A$ (m$^2$) | 3.02 | 86.13 | 120.02 | 29,937.71 | 333.90 |
| $P$ (m) | 7.70 | 41.28 | 44.13 | 1711.41 | 26.23 |
| $l$ (m) | 2.27 | 14.37 | 15.67 | 550.76 | 10.74 |
| (m) | 1.57 | 8.56 | 9.40 | 278.67 | 5.46 |
| $\phi$ (°) | 0 | 78.98 | 83.23 | 179.98 | 53.04 |
| $CI$ | 0.03 | 0.69 | 0.68 | 0.99 | 0.09 |
| $ELG$ | 1.00 | 1.58 | 1.71 | 41.29 | 0.63 |
| $REC$ | 0.23 | 0.98 | 0.93 | 1.00 | 0.10 |
| $H$ (m) | 1.88 | 7.75 | 7.56 | 64.60 | 2.35 |
| $\bar{H}$ (m) | 1.70 | 6.31 | 6.20 | 56.14 | 1.89 |
| $V$ (m$^3$) | 15.84 | 550.51 | 812.36 | 348,017.50 | 3254.18 |
| Volume per floor $VPF$ (m$^3$) | 6.32 | 390.23 | 584.75 | 139,207 | 2770.00 |

64-bit operating system. The total time for the EMST generation was 2207 s for the 103,901 building objects, including the calculation of the homogeneity index. It should be noted that approximately 60% of the time cost (1347 s) was spent in the MST generation using Prim's algorithm.

The basic MST in EMST was generated based on the boundary distance between building objects. Figure 5(a) shows the MST result for the entire study area and Figure 5 (b) zooms over the area marked by the yellow box shown in Figure 5(a). From Figure 5 (a), we can see that the buildings are located unevenly across the region. Most of the buildings are located in the northeastern and south shore. The western part of the region has the lowest building density with only a few MST exist. With a close look at Figure 5(b), most of the buildings in the same block link together and the MST extend to adjacent blocks by connecting the closest buildings between these blocks. The entire MST consists of 103,901 nodes (represented by the centroid points of buildings) and 103,900 edges, which are weighted by the boundary distance between the corresponding buildings. Statistics (not shown here) reveal that the MST edges have an average weight of 6.52 m, which indicates that the buildings in the study area are located very close to each other, and the average building density is very high.

As explained Section 3.3, we used the Gestalt theory-based partition method to subdivide the basic MST in EMST into different locally connected subsets. By setting the parameters properly, the MST shown in Figure 5(a) was partitioned into a number of subgraphs. The partition result is shown in Figure 6(a) and Figure 6(b) zooms over the yellow box area in Figure 6(a) to show a close look at the MST partition result. Each subgraph is colored differently in Figure 6. In total, 4505 subgraphs were derived. From Figure 6(a), a variety of structures can be revealed across the study area. The subgraphs tend to be smaller on the south shore, and the subgraphs in the north region tend to be larger. The largest subgraph was found in the north of the study area (the area covered by the red box in Figure 6(a)), which contains 7964 buildings.
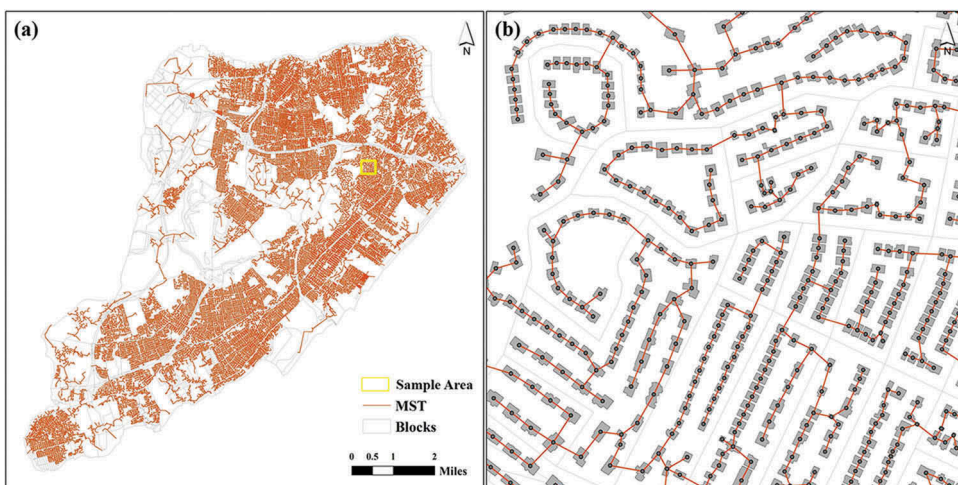


**Figure 5.** The minimum spanning tree for the building objects in Staten Island. (a) MST for the entire island; (b) MST for the area located in the yellow box shown in (a).

**Figure 6.** The partitioned minimum spanning tree for the building objects in Staten Island. (a) The partitioned MST for the entire island; (b) the partitioned MST for the area marked by the yellow box in (a).

By performing a statistical analysis on the subgraphs shown in Figure 6(a), we found that over a quarter of the subgraphs comprise less than 10 buildings and only 95 subgraphs comprise more than 100 buildings (see Figure 7(a)). The average building boundary distance within each subgraph ranges from 0 to 25 m (Figure 7(b)). Approximately 50% of the subgraphs have an average building boundary distance within the range of 3–7 m. The distribution of the average boundary distance is obviously skewed to the left, which indicates a compact building environment and high-density morphologies in the study area. Interestingly, we found that approximately half of the subgraphs are located perfectly in their corresponding blocks (see Figure 6 (b)), especially in the central-eastern part of the island. It is easy to imagine that the building boundary distance between the buildings in the same block is significantly smaller than the distance between the buildings in different blocks. Therefore, the edges connecting the buildings in different blocks will be cut off. Thus, it can be seen that many subgraphs in our study area are located in their blocks. In turn, our method can be used to identify the extent of blocks in the study area to some extent.

Taking the largest subgraph (located within the red box in Figure 6(a)) as an example, we summarized its UBCs statistics in Table 3. The buildings in the largest subgraph have an average area of approximately 127 m$^2$ and an average perimeter of 45 m. The area and perimeter of the buildings in this area are spread out over a very wide range with a high standard deviation. From the statistics of shape attributes, especially the *REC* index, which has an average value smaller than the median, we can conclude that most of the buildings in this region tend to be have a rectangular shape. These buildings have an average height of 7.38 m, which occupies an average volume of 821 m$^3$ and an average volume of 426 m$^3$ per floor. If we compare Table 3 with Table 2, most of the statistics are very similar, indicating that this area can treated as a typical epitome of the entire study area.
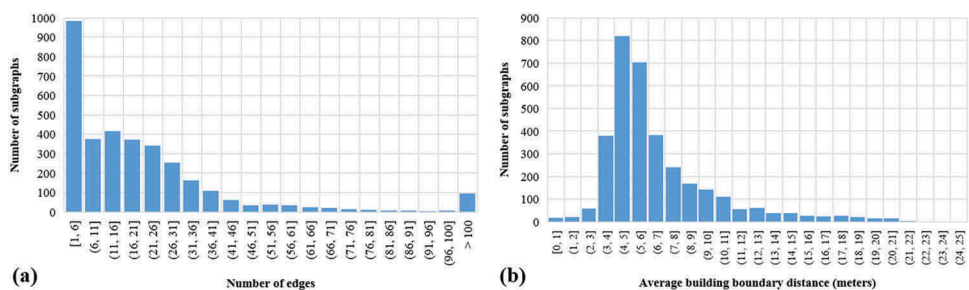
**Figure 7.** Statistical distribution of subgraphs. (a) Distribution of size; (b) distribution of average building boundary distance.

**Table 3.** Summary statistics on urban building characteristics for the largest subgraph.

| UBCs | Min | Median | Mean | Max | Standard deviation |
|---|---|---|---|---|---|
| $A$ (m$^2$) | 5.56 | 90.75 | 126.79 | 15,552.19 | 315.68 |
| $P$ (m) | 9.46 | 41.77 | 44.82 | 808.39 | 29.15 |
| $l$ (m) | 2.54 | 13.58 | 14.22 | 240.89 | 8.98 |
| $w$ (m) | 2.18 | 6.91 | 8.01 | 133.52 | 5.11 |
| $\phi$ (°) | 0 | 73.46 | 76.33 | 179.98 | 54.80 |
| $CI$ | 0.12 | 0.67 | 0.67 | 0.94 | 0.09 |
| $ELG$ | 1.00 | 1.73 | 1.82 | 7.00 | 0.61 |
| $REC$ | 0.29 | 0.98 | 0.94 | 1.00 | 0.09 |
| $H$ (m) | 2.10 | 8.33 | 7.38 | 30.15 | 2.12 |
| $\bar{H}$ (m) | 1.76 | 6.33 | 5.90 | 22.72 | 1.91 |
| $V$ (m$^3$) | 20.14 | 573.87 | 821.98 | 97,992.04 | 2278.85 |
| $VPF$ (m$^3$) | 7.06 | 256.80 | 416.34 | 97,992.04 | 1816.40 |

After partitioning the MST, the characterization of local patterns was performed. Table 4 reports LISA categories for all edges in the subgraphs with respect to different UBCs. From Table 4, most of the MST edges are located within the heterogeneous pattern and a very large portion of them have a nonsignificant local Moran's $I$. A special weight is given to four UBCs, including the orientation, compactness index, height and average height. Almost half of the MST edges are located within the homogeneous pattern in our study area concerning these four UBCs. This indicates that the most of the buildings are tightly connected with similar orientation, compactness and height.

**Table 4.** Number of edges per local patterns for all the UBCs.

| | Homogeneous | | Heterogeneous | | |
|---|---|---|---|---|---|
| UBCs | HH | LL | HL | LH | N.S. |
| $A$ (m$^2$) | 1754 | 0 | 202 | 41 | 97,400 |
| $P$ (m) | 4263 | 7295 | 1256 | 725 | 85,858 |
| $l$ (m) | 4545 | 9287 | 1570 | 992 | 83,003 |
| $w$ (m) | 6093 | 13,294 | 2655 | 1216 | 76,139 |
| $\phi$ (°) | 20,293 | 23,027 | 8450 | 6001 | 41,626 |
| $CI$ | 16,284 | 9695 | 4595 | 5500 | 63,323 |
| $L$ | 9676 | 4677 | 3297 | 4677 | 69,229 |
| $REC$ | 13,024 | 8116 | 3499 | 4781 | 69,977 |
| $H$ (m) | 12,353 | 14,994 | 6741 | 4696 | 60,613 |
| $\bar{H}$ (m) | 12,341 | 15,912 | 6330 | 4004 | 60,810 |
| $V$ (m$^3$) | 1222 | 0 | 127 | 27 | 98,021 |
| $VPF$ (m$^3$) | 787 | 0 | 86 | 11 | 96,787 |

Heterogeneous patterns are mainly found according to area, perimeter, length, width, volume and volume per floor, indicating buildings are varying in these characteristics at the local scale and there's no significant pattern that can be identified.

Figure 8 shows the local pattern characterization for the largest subgraph in our study area. These maps are consistent with the summary statistics in Table 4. The distribution of local patterns of area, perimeter, length and width is very similar, with HH patterns mainly
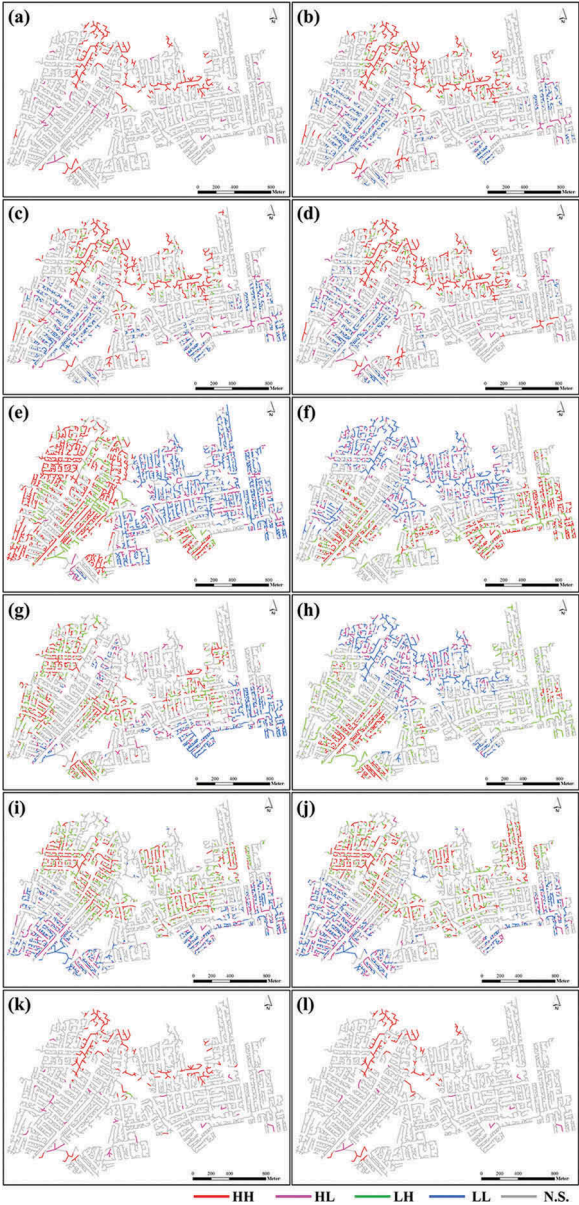


**Figure 8.** The local patterns identified for the largest subgraph with respect to (a) area; (b) perimeter; (c) length; (d) width; (e) orientation; (f) compactness index; (g) elongatedness; (h) rectangularity; (i) height; (j) average height; (k) volume; and (l) average volume per floor.

distributed in the northern part and LL patterns located in the southern part. A large proportion of the nonsignificant pattern was found in reference to the area, volume and volume per floor. For the orientation, a strong spatial pattern can be observed: buildings in the west have high orientation angles, whereas low orientation angles are found in the east. Overall, our results demonstrate the ability of our EMST method for identifying local patterns from different building characteristics at building-unit level.

Finally, we calculated the homogeneity index for the largest subgraph from the local patterns shown in Figure 8. The distribution of the homogeneity index is shown in Figure 9. Approximately 20% of the edges in Figure 9 have a homogeneity index of 0, which are scattered across the area. The buildings associated with these edges are homogeneous only in spatial distance. Four sites (marked with red boxes in Figure 9) with high homogeneity index are identified. The buildings in these four areas are homogeneous both in spatial distance measures and most of the morphological characteristics. In the homogeneity index map, building pattern is treated as a set of close buildings which are connected by the edges with similar homogeneity index. These edges have two indications. On the one hand, the buildings connected by these edges have a well-organized spatial distribution. On the other hand, the homogeneity index of these edges indicates that the buildings have some similarities in their morphological properties. The distribution of the homogeneity index shows an overall building pattern, which takes both spatial distance and morphological characteristics into account.

Figure 10 shows the building patterns for the four sites marked in Figure 9. From the point of spatial arrangements, both the regular (highly organized) building patterns and irregular (unorganized) building patterns are revealed from Figure 10. Sites **A** and **C** tend to



**Figure 9.** The distribution of the homogeneity index.

**Figure 10.** The building patterns and Google Map images for (a) site A; (b) site B; (c) site C; and (d) site D.

have irregular patterns as the MST edges are distributed unevenly in these two sites and the homogeneity index vary considerably. Similarly, Sites **B** and **D** tend to have regular patterns as the majority of the MST edges have a linear distribution and most of the buildings in these two sites have a similar homogeneity index. We also noticed that the homogeneity index in sites **A** and **C** is higher than that in sites **B** and **D**, indicating that the UBCs among the buildings in sites **A** and **C** are much more similar than that in sites **B** and **D**. This suggests that the urban structure types are different in these four sites. According to the study by Steiniger *et al.* (2008) and Meinel *et al.* (2009), site **A** is more likely to be an industry/

commercial area due to the large 3D morphological measures and low building density, while site **C** tends to be a multifamily residential area due to the relative lower building volume and height compared with site **A**. Sites **B** and **D** are more likely to be single-family residential areas due to the small building volume, low building height, high building density and the regular spatial arrangement. To clarify our judgments, we captured the corresponding satellite images (see Figure 10) for the four sites from Google Maps. Site **A** is a commercial area with a lot of shopping malls and restaurants visible from the satellite image; sites **B** and **D** are single-family residential areas with many single-family homes situated around; site **C** is a mixed functional area composed of some high-rise apartments and a small commercial zone. These Google Map images confirmed our judgments. It can be argued that the buildings in industry/commercial areas and multifamily residential areas are easily distinguishable from their neighbors, which makes them group into an HH pattern. While the buildings located in single-family residential areas are more likely to have various and random morphological characteristics, they tend to have a heterogeneous pattern at local scale. Therefore, the urban structure type can be revealed by carefully examining the homogeneity index and the UBCs.

## 5. Discussion

As one of the most crucial components of urban structures and functions, building patterns are essential for us to understand the urban space and built environments. Different buildings have different vertical and horizontal morphologies, making the urban morphology more complex. When building pattern is the subject of analyses, it is practical to treat buildings as spatial units for urban morphology analysis. Many studies (Regnauld 2001, Christophe and Ruas 2002, Li *et al.* 2004, Yoshida and Omae 2005, Steiniger *et al.* 2008) argue that the combination of spatial relations in geographical space and the morphological properties are likely to be a better way to reveal urban local forms. In the exploitation of the potential of 2D and 3D building characteristics as properties of urban morphology, we developed the EMST method to identify local building patterns. The approach presented in this study can offer insight into a deeper understanding of urban morphology.

Our EMST data structure is a formally defined and highly flexible method, which has various advantages over previous studies. First, we treated buildings as objects which are more in line with the way for interpreting the urban scene by humans or computers. The building objects take a great deal of information such as building volume, height and shape. These meaningful building objects are the only input of the EMST, which is critical to identify building patterns with a reliable degree of consistency and accuracy. Second, although the design of our method is based on the basic structure of MST, the EMST not only inherits the inherent properties of the basic MST but also involves new sets, relations and functions. Compared with the basic MST, four new sets are added to extend its ability for analyzing local building patterns. With respect to spatial relations, the proximity relation defined by the boundary distance was considered in our study. The proximity measuring the distance between buildings' boundaries is more reliable than the distance between buildings' centroid points in previous studies. Two functions, partitioning and spatial autocorrelation, are employed to identify the local patterns through both graph cutting and local statistics. Combined with these new sets, relations,

and functions, the EMST can assist in enhancing the understanding of local building patterns from various perspectives. Third, the homogeneity index summarizes all homogeneous and heterogeneous units into a single value to quantify the local building patterns. The distribution of homogeneity index allows us to characterize building patterns in a natural and intuitive way.

Compared with the existing methods, our new method characterizes not only the connectivity and proximity relations of buildings but also the structural and morphological characteristics at the building-unit level. Most existing methods only focused on one of these aspects, lacking the ability to identify comprehensive local building patterns. Here, we implemented the method proposed by Caruso et al. (2017) and the extracted patterns are shown in Figure 11. Their approach identified the building patterns solely based on the distance between the centroids of buildings. Therefore, the connections between buildings are very different from our results shown in Figure 10, especially the buildings in



**Figure 11.** The building patterns extracted by the method of Caruso et al. (2017): (a) site A; (b) site B; (c) site C; and (d) site D.

sites **A** and **C**. The connections in the EMST are more consistent with human intuition. Due to the high density of building distribution in our study area, their approach only identified 59 subgraphs with a fixed distance threshold, and the largest subgraph contained 103,713 buildings (almost all the buildings in the study area). Therefore, it appears that their approach could not identify local building groups in such a complex building environment. Moreover, their approach could not express the morphological and functional characteristics of these local units. In addition, Regnauld (2001) used MST to group buildings based on the typification principle. Although each group of buildings is attached with essential geographical information, they were all used for building generalization. Dogrusoz and Aksoy (2007a) classified urban buildings into organized or unorganized groups without recognizing the structural characteristics. Unlike these existing studies, EMST is a comprehensive and systematic method for characterizing local urban patterns in a complex building environment.

Two fundamental laws of GIScience have been illustrated in our study. The Tobler's first law (Tobler 1970) was used in the process of EMST generation and partition to ensure the homogeneity of distance among neighboring buildings at a local scale. The subgraph set *C* in EMST is a set of building groups which keep the homogeneity of boundary distance. Based on the subgraph set *C*, we observed the heterogeneity of building patterns by using the law of heterogeneity which was described as the second law of GIScience according to Goodchild (2004). At the building-unit level, spatial heterogeneity of building patterns could be discovered by comparing the UBCs of each building. In our study, we recognized the local building patterns as set *P* in EMST by using spatial autocorrelation analysis. Steiniger *et al.* (2008) also argued that these two fundamental laws of GIScience are the basic rules to understand the development of urban structures.

The results presented in our study suggest that local patterns of different building characteristics can be distinguishable through our proposed EMST. However, the efficiency and accuracy of local patterns identified by our EMST method may be influenced by several factors when applying it to other areas. The first issue should be treated with a degree of caution is the LiDAR data. It is challenging to extract the 3D UBCs of buildings from LiDAR data if buildings are shaded by trees. Besides, the spatial resolution and vertical accuracy of LiDAR data can affect the 3D UBCs extraction. Second, the option of MST edge partition ratio and the step length could influence the local pattern identification result. The selection of a small edge partition ratio and the step length may generate an excessive amount of small subgraphs. Otherwise, only several very large subgraphs will be generated. Producing too small and large subgraphs (patterns) are meaningless in urban studies (Cetinkaya *et al.* 2015). As a general guideline, one can get a satisfactory result by using the trial and error approach. Another concern is the storage and operational efficiency of the EMST. When working on large datasets, the requirements on computation power and computer memory will stack up rapidly. In this case, building indexes for the logical sets in EMST would be effective, and the subsection processing technology can also be applied to improve the efficiency.

## 6. Conclusion

Measuring urbanization patterns, especially the local patterns of buildings, is essential for urban planning and environmental sustainability. Most of the previous studies evaluated the urban forms at the administrative unit level, which is too coarse to

characterize local urban patterns. Moreover, few studies have been reported to integrate both 2D and 3D UBCs as potential indicators for characterizing local building patterns at building-unit level. In this study, we presented an innovative and simple EMST method for automatically identifying local building patterns. The buildings were conceptualized and treated as building objects to collect various morphologic information, which provides a better understanding of the local building environment. Based on the building footprint data and high-resolution LiDAR data, the 2D and 3D UBCs can be calculated. The EMST is then established to represent and describe the spatial proximity relations and UBCs. By applying the Gestalt theory-based graph partition method and spatial autocorrelation technique, various homogeneous and heterogeneous patterns can be characterized and identified by fusing the 2D and 3D UBCs. The case study results demonstrate the ability of the proposed method for characterizing building patterns at a local level.

Our EMST approach can identify and characterize meaningful and functional local groups of building in an unorganized building environment. These local groups are attached with abundant 2D/3D morphological indicators which can be used to estimate population in urban districts by building relationships the census data. The structures of local building forms extracted by the EMST can be considered as structurally homogeneous regions to derive urban structure types (Walde *et al.* 2014), urbanization processes (Caruso *et al.* 2017) and further use to assess urbanization dynamics (Lowry and Lowry 2014) by integrating local knowledge. Besides, our method has a strong advantage for studying both ecological impacts of urbanization patterns or for designing urban planning scenarios since our approach based on the building-unit level. For example, we can use the EMST output to guide and prioritize the construction plans of urban infrastructure (e.g. transport network), minimizing the negative impacts on urban ecological corridors.

Our EMST method allows for recognizing local connectivity and patterns of urban buildings from multiple views. Although the building boundary distance can serve as a basic but important indicator for inferring the local building connection, it is still challenging to evaluate and measure the patterns at a local level due to the lack of morphologic information of buildings. Our EMST establishes the direct relationships between detailed UBCs and the spatial distribution of buildings. In this way, both morphological and spatial indicators are readily available to infer the local patterns. Nevertheless, the attempt made in this study still needs certain enhancements for further developments of analyses on urban morphology. Further insights on how to extract the functions and structures of urban buildings from EMST can be investigated. Furthermore, our EMST method can be extended and applied to a wide range of studies and applications related to urban morphology and structures.

## Acknowledgments

## Disclosure statement

## ORCID

Bailang Yu  http://orcid.org/0000-0001-5628-0003
Qiusheng Wu  http://orcid.org/0000-0001-5437-4073

## References

Anders, K.-H., 2006. Grid typification. *In*: A. Riedl, W. Kainz, and G.A. Elmes, eds. *Progress in Spatial data handling: 12th international symposium on spatial data handling*. Berlin, Heidelberg: Springer Berlin Heidelberg, 633–642.

Anders, K.-H., Sester, M., and Fritsch, D., 1999. Analysis of settlement structures by graph-based clustering. *In*: W. Forstner, C.-E. Liedtke, and J. Buckner eds. *Proceedings of the Semantic Modelling for the Acquisition of Topographic Information from Images and Maps Conference (SMATI'99)*. Munich, Germany: Deutsche Forschungsgemeinschaft, 41–49.

Anselin, L., 1995. Local Indicators of Spatial Association—LISA. *Geographical Analysis*, 27 (2), 93–115. doi:10.1111/j.1538-4632.1995.tb00338.x

Antonarakis, A.S., Richards, K.S., and Brasington, J., 2008. Object-based land cover classification using airborne LiDAR. *Remote Sensing of Environment*, 112 (6), 2988–2998. doi:10.1016/j.rse.2008.02.004

Assunção, R.M., *et al*., 2006. Efficient regionalization techniques for socio-economic geographical units using minimum spanning trees. *International Journal of Geographical Information Science*, 20 (7), 797–811. doi:10.1080/13658810600665111

Baud, I., *et al*., 2010. Understanding heterogeneity in metropolitan India: the added value of remote sensing data for analyzing sub-standard residential areas. *International Journal of Applied Earth Observation and Geoinformation*, 12 (5), 359–374. doi:10.1016/j.jag.2010.04.008

Benz, U.C., *et al*., 2004. Multi-resolution, object-oriented fuzzy analysis of remote sensing data for GIS-ready information. *ISPRS Journal of Photogrammetry and Remote Sensing*, 58 (3–4), 239–258. doi:10.1016/j.isprsjprs.2003.10.002

Berger, C., *et al*., 2017. Spatio-temporal analysis of the relationship between 2D/3D urban site characteristics and land surface temperature. *Remote Sensing of Environment*, 193, 225–243. doi:10.1016/j.rse.2017.02.020

Brodu, N. and Lague, D., 2012. 3D terrestrial lidar data classification of complex natural scenes using a multi-scale dimensionality criterion: applications in geomorphology. *ISPRS Journal of Photogrammetry and Remote Sensing*, 68, 121–134. doi:10.1016/j.isprsjprs.2012.01.006

Burnett, C. and Blaschke, T., 2003. A multi-scale segmentation/object relationship modelling methodology for landscape analysis. *Ecological Modelling*, 168 (3), 233–249. doi:10.1016/S0304-3800(03)00139-X

Cadenasso, M.L., Pickett, S.T., and Schwarz, K., 2007. Spatial heterogeneity in urban ecosystems: reconceptualizing land cover and a framework for classification. *Frontiers in Ecology and the Environment*, 5 (2), 80–88. doi:10.1890/1540-9295(2007)5[80:SHIUER]2.0.CO;2

Carmona, M., *et al*., 2003. *Public places, urban spaces: the dimensions of urban design*. Oxford: Architectural Press.

Caruso, G., Hilal, M., and Thomas, I., 2017. Measuring urban forms from inter-building distances: combining MST graphs with a Local Index of Spatial Association. *Landscape and Urban Planning*, 163, 80–89. doi:10.1016/j.landurbplan.2017.03.003

Cetinkaya, S., Basaraner, M., and Burghardt, D., 2015. Proximity-based grouping of buildings in urban blocks: a comparison of four algorithms. *Geocarto International*, 30 (6), 618–632. doi:10.1080/10106049.2014.925002

Chen, Q., *et al.*, 2006. Isolating individual trees in a savanna woodland using small footprint Lidar data. *Photogrammetric Engineering & Remote Sensing*, 72 (8), 923–932. doi:10.14358/PERS.72.8.923

Chen, Y., *et al.*, 2009. Hierarchical object oriented classification using very high resolution imagery and LIDAR data over urban areas. *Advances in Space Research*, 43 (7), 1101–1110. doi:10.1016/j.asr.2008.11.008

Christophe, S. and Ruas, A., 2002. Detecting building alignments for generalisation purposes. *In*: D. E. Richardson and P. Van Oosterom, eds. *Advances in spatial data handling: 10th international symposium on spatial data handling*. Berlin, Heidelberg: Springer Berlin Heidelberg, 419–432.

de Almeida, J.-P., Morley, J.G., and Dowman, I.J., 2013. A graph-based algorithm to define urban topology from unstructured geospatial data. *International Journal of Geographical Information Science*, 27 (8), 1514–1529. doi:10.1080/13658816.2012.756881

Deng, M., *et al.*, 2011. An adaptive spatial clustering algorithm based on delaunay triangulation. *Computers, Environment and Urban Systems*, 35 (4), 320–332. doi:10.1016/j.compenvurbsys.2011.02.003

Dogrusoz, E. and Aksoy, S., 2007a. Modeling urban structures using graph-based spatial patterns. *In*: Tsang, L. ed. *IEEE International Geoscience and Remote Sensing Symposium*. Barcelona, Spain: IEEE, 4826–4829.

Dogrusoz, E. and Aksoy, S., 2007b. Modeling urbanization using building patterns. *In*: Barkana, A. ed. *IEEE 15th signal processing and communications applications*. Eskisehir, Turkey: IEEE, 1–4.

Donnay, J.-P., Barnsley, M.J., and Longley, P.A., 2003. *Remote sensing and urban analysis: GISDATA 9*. New Fetter Lane, London: CRC Press.

Du, S., *et al.*, 2016. Extracting building patterns with multilevel graph partition and building grouping. *ISPRS Journal of Photogrammetry and Remote Sensing*, 122, 81–96. doi:10.1016/j.isprsjprs.2016.10.001

Fan, C. and Myint, S., 2014. A comparison of spatial autocorrelation indices and landscape metrics in measuring urban landscape fragmentation. *Landscape and Urban Planning*, 121, 117–128. doi:10.1016/j.landurbplan.2013.10.002

Gans, H.J., 1961. The balanced community: homogeneity or heterogeneity in residential areas? *Journal of the American Institute of Planners*, 27 (3), 176–184. doi:10.1080/01944366108978452

Goodchild, M.F., 2004. The validity and usefulness of laws in geographic information science and geography. *Annals of the Association of American Geographers*, 94 (2), 300–303. doi:10.1111/j.1467-8306.2004.09402008.x

Grinias, I., Panagiotakis, C., and Tziritas, G., 2016. MRF-based segmentation and unsupervised classification for building and road detection in peri-urban areas of high-resolution satellite images. *ISPRS Journal of Photogrammetry and Remote Sensing*, 122, 145–166. doi:10.1016/j.isprsjprs.2016.10.010

Han, J., Lee, J.-G., and Kamber, M., 2009. An overview of clustering methods in geographic data analysis. *In*: H.J. Miller, ed. *Geographic data mining and knowledge discovery*. 2nd ed. Boca Raton, FL: CRC Press, 149–188.

Huang, Y., *et al.*, 2015. Estimating roof solar energy potential in the downtown area using a GPU-accelerated solar radiation model and airborne LiDAR data. *Remote Sensing*, 7 (12), 17212–17233.

Li, Z., *et al.*, 2004. Automated building generalization based on urban morphology and Gestalt theory. *International Journal of Geographical Information Science*, 18 (5), 513–534.

Liu, H., *et al.*, 2010. An object-based conceptual framework and computational method for representing and analyzing coastal morphological changes. *International Journal of Geographical Information Science*, 24 (7), 1015–1041.

Liu, L. and Lim, S., 2016. A framework of road extraction from airborne lidar data and aerial imagery. *Journal of Spatial Science*, 61 (2), 263–281.

Lowry, J.H. and Lowry, M.B., 2014. Comparing spatial metrics that quantify urban form. *Computers, Environment and Urban Systems*, 44, 59–67.

Meinel, G., Hecht, R., and Herold, H., 2009. Analyzing building stock using topographic maps and GIS. *Building Research & Information*, 37 (5–6), 468–482.

Mesev, V., 2005. Identification and characterisation of urban building patterns using IKONOS imagery and point-based postal data. *Computers, Environment and Urban Systems*, 29 (5), 541–557.

Miliaresis, G. and Kokkas, N., 2007. Segmentation and object-based classification for the extraction of the building class from LIDAR DEMs. *Computers & Geosciences*, 33 (8), 1076–1087.

Neuwirth, C., Hofer, B., and Schaumberger, A., 2016. Object view in spatial system dynamics: a grassland farming example. *Journal of Spatial Science*, 61 (2), 367–388.

Niemeyer, J., Rottensteiner, F., and Soergel, U., 2014. Contextual classification of lidar data and building object detection in urban areas. *ISPRS Journal of Photogrammetry and Remote Sensing*, 87, 152–165.

Nordbeck, S., 1971. Urban allometric growth. *Geografiska Annaler. Series B, Human Geography*, 53 (1), 54–67.

Prim, R.C., 1957. Shortest connection networks and some generalizations. *The Bell System Technical Journal*, 36 (6), 1389–1401.

Ratti, C., 2004. Space syntax: some Inconsistencies. *Environment and Planning B: Planning and Design*, 31 (4), 487–499.

Regnauld, N., 1996. Recognition of building clusters for generalization. *In*: M.J. Kraak and M. Molenaar. eds. *Proceedings of the 7th International Symposium on Spatial Data Handling*. Delft, the Netherlands: TU Delft, 185–198.

Regnauld, N., 2001. Contextual building typification in automated map generalization. *Algorithmica*, 30 (2), 312–333.

Sohn, G. and Dowman, I., 2007. Data fusion of high-resolution satellite imagery and LiDAR data for automatic building extraction. *ISPRS Journal of Photogrammetry and Remote Sensing*, 62 (1), 43–63.

Steiniger, S., et al., 2008. An approach for the classification of urban building structures based on discriminant analysis techniques. *Transactions in GIS*, 12 (1), 31–59.

Sternberg, R.J. and Sternberg, K., 2011. *Cognitive psychology*. 6th ed. Belmont, CA: Wadsworth Publishing. February 8, 2011.

Taubenböck, H., et al., 2010. Object-based feature extraction using high spatial resolution satellite data of urban areas. *Journal of Spatial Science*, 55 (1), 117–132.

Tobler, W.R., 1970. A computer movie simulating urban growth in the Detroit region. *Economic Geography*, 46 (sup1), 234–240.

United States Census Bureau, 2016. Community facts – Staten Island borough, Richmond County, New York. *United States Census Bureau. Retrieved March*, 24, 2016.

Urban, D. and Keitt, T., 2001. Landscape connectivity: a graph-theoretic perspective. *Ecology*, 82 (5), 1205–1218.

Walde, I., et al., 2014. From land cover-graphs to urban structure types. *International Journal of Geographical Information Science*, 28 (3), 584–609.

Whitehand, J.W.R., 1992. Recent advances in urban morphology. *Urban Studies*, 29 (3–4), 619–636.

Wu, B., et al. 2012. Voxel-based marked neighborhood searching method for identifying street trees using vehicle-borne laser scanning data. *In*: Q. Weng, et al. eds. *Proceedings of the second international workshop on Earth Observation and Remote Sensing Applications (EORSA)*. Shanghai, China: IEEE, 327–331.

Wu, B., et al., 2013. A voxel-based method for automated identification and morphological parameters estimation of individual street trees from mobile laser scanning data. *Remote Sensing*, 5 (2), 584–611.

Wu, B., et al., 2016a. Automated extraction of ground surface along urban roads from mobile laser scanning point clouds. *Remote Sensing Letters*, 7 (2), 170–179.

Wu, B., *et al*., 2016b. Individual tree crown delineation using localized contour tree method and airborne LiDAR data in coniferous forests. *International Journal of Applied Earth Observation and Geoinformation*, 52, 82–94.

Wu, B., *et al*., 2017. A graph-based approach for 3D building model reconstruction from airborne LiDAR point clouds. *Remote Sensing*, 9 (1), 92.

Wu, S.-S., Qiu, X., and Wang, L., 2005. Population estimation methods in GIS and remote sensing: a review. *GIScience & Remote Sensing*, 42 (1), 80–96.

Yoshida, H. and Omae, M., 2005. An approach for analysis of urban morphology: methods to derive morphological properties of city blocks by using an urban landscape model and their interpretations. *Computers, Environment and Urban Systems*, 29 (2), 223–247.

Yu, B., *et al*., 2009. Investigating impacts of urban morphology on spatio-temporal variations of solar radiation with airborne LIDAR data and a solar flux model: a case study of downtown Houston. *International Journal of Remote Sensing*, 30 (17), 4359–4385.

Yu, B., *et al*., 2010. Automated derivation of urban building density information using airborne LiDAR data and object-based method. *Landscape and Urban Planning*, 98 (3–4), 210–219.

Yu, B., *et al*., 2014. Object-based spatial cluster analysis of urban landscape pattern using nighttime light satellite images: a case study of China. *International Journal of Geographical Information Science*, 28 (11), 2328–2355.

Yu, S., *et al*., 2016. View-based greenery: A three-dimensional assessment of city buildings' green visibility using Floor Green View Index. *Landscape and Urban Planning*, 152, 13–26.

Yu, W., *et al*., 2017. The analysis and measurement of building patterns using texton co-occurrence matrices. *International Journal of Geographical Information Science*, 31 (6), 1079–1100.

Zhang, K., Yan, J., and Chen, S.C., 2006. Automatic construction of building footprints from airborne LIDAR data. *IEEE Transactions on Geoscience and Remote Sensing*, 44 (9), 2523–2533.

Zhang, X., *et al*., 2013a. Building pattern recognition in topographic data: examples on collinear and curvilinear alignments. *GeoInformatica*, 17 (1), 1–33.

Zhang, X., *et al*., 2013b. Automated evaluation of building alignments in generalized maps. *International Journal of Geographical Information Science*, 27 (8), 1550–1571.